CrystEngComm

Accepted Manuscript

ROYAL SOCIETY OF CHEMISTRY

www.rsc.org/crystengcomm

Adsorption and UV/Visible photocatalytic performance of BiOI for methyl orange, Rhodamine B and methylene blue: Ag and Ti-loading effects

Yohan Park,[1] Yulyi Na,[1] Debabrata Pradhan,[2] Bong-Ki Min,[3] and Youngku Sohn[1,*]

[1]Department of Chemistry, Yeungnam University, Gyeongsan 712-749, Republic of Korea

[2]Materials Science Centre, Indian Institute of Technology, Kharagpur 721 302, W.B., India

[3] Instrumental Analysis Center, Yeungnam University, Gyongsan 712-749, Republic of Korea

Abstract

We synthesized echinoid-like BiOI microspheres with various doped concentrations of Ag (0.1, 1.0, 5.0, 10.0 mol%) and Ti (1.0, 5.0, 10.0, 30.0, 50.0 mol%) in ethylene glycol and then examined their fundamental properties by scanning electron microscopy, transmission electron microscopy, X-ray diffraction analysis, UV-visible absorption, FT-IR, Raman, photoluminescence, and Brunauer-Emmett-Teller (BET) surface area measurements. We also measured the adsorption and photocatalytic dye-degradation performance of the catalysts using methyl orange (MO), Rhodamine B (RhB) and methylene blue (MB). The adsorption performance was found to be in the order of MO < RhB < MB, and to depend somewhat upon Ag and Ti-loadings. MO was degraded in the order of BiOI < Ag-BiOI < Ti-BiOI under UV and visible light irradiation, while the degradation of RhB was in the order of Ag-BiOI ≈ Ti-BiOI << BiOI, and Ag-BiOI < BiOI < Ti-BiOI, respectively. MB showed poor photodegradation under UV and visible light. Finally, we used an indirect chemical probe method with active species scavengers and photoluminescence spectroscopy to clarify the dye-sensitized photodegradation mechanism. In the mechanism, $\bullet O_2^-$ and h^+ were active species under visible light irradiation. No •OH radicals were found by luminescence spectroscopy.

* Corresponding author e-mail: youngkusohn@ynu.ac.kr

Tel: +82-53-810-2354; Fax:+82-53-810-4613

Key words: BiOI; Doping; Adsorption; Photodegradation; Dye-sensitized

1. Introduction

Water treatments and impurity removal aided by adsorption and photocatalysis using a catalyst are very important. Bismuth oxyhalides (BiOX, X=Cl, Br and I) have recently been extensively investigated for use as adsorbents and photocatalysts for the removal of unwanted pollutants.[1-47] Since adsorption and photocatalytic performance are commonly determined by morphology (e.g., sizes and crystal facets) and composition, many studies have been conducted to tailor morphology and synthesize hybrid materials. Two morphologies of 3D-echinoid-like (or 3D-hierarchical flower-like) and 2D-sheets (or 2D-plates) have commonly been obtained and reported for BiOX. In many tested systems such as those that evaluate dye removal, the 3D BiOX structure has shown much higher adsorption and photocatalytic activities than the 2D structure.[35] Recently, more extensive research has focused on designing hybrid materials with BiOI to further enhance catalytic activity under visible light irradiation. The reported hybrid materials include AgI/BiOI [1,2,4,47] Ag/AgI/BiOI,[10,11] Ag/BiOI,[29,30] TiO_2/BiOI,[31,35,36] MnO_x–BiOI,[3] BiOI/$ZnSn(OH)_6$,[5] BiOI/Bi_2WO_6,[6,7] BiOI/$BiPO_4$,[13] Ag_3PO_4/BiOI,[18] Bi/BiOI,[19] BiOI–MWCNT,[21] BiOI/n-$ZnTiO_3$[20] BiOI/BiOX,[22,24,26,37,41,42] Bi_2S_3/BiOI,[27] $Bi_2O_2CO_3$/BiOI,[28] BiOI/B_2O_3,[38,39] ZnO/BiOI,[40] and Pt/BiOI.[46] The heterojunction material commonly enhances visible light absorption and further facilitates good electron-hole transport and separation, which results in good removal of impurities by photoabsorption. When a n-type (e.g., ZnO and TiO_2) material with a higher band gap (3.0 – 4.0 eV) is junctioned with p-type BiOI with a lower band gap of ~1.8 eV, visible light irradiation creates an electron and a hole in the conduction and valence bands in BiOI, respectively.[35,36,40] The electrons are then efficiently transferred to the conduction band of the p-type material, leaving the hole in the valence band of BiOI. This process facilitates the electron-hole pair separation without recombination. Metallic nanoparticles such as Ag have been reported to facilitate the capture of photogenerated electrons by surface oxygen to form superoxide ($\cdot O_2^-$) radicals, which act as oxidants[30] Cheng et al. demonstrated that AgI/BiOI hierarchical hybrids show much higher photocatalytic 2,4-dichlorophenol decomposition than unhybridized BiOI, and the activity was shown to decrease with decreasing Ag nanoparticle size.[1] It has been reported that photoinduced holes in AgI/BiOI hybrid materials are the main factor responsible for degradation of organic pollutants.[47] Major

active intermediate species include hydroxyl radicals (•OH), superoxide radicals ($•O_2^-$), electrons (e^-) and holes (h^+). DMPO (5,5-dimethyl-1-pyrroline N-oxide) EPR (electron paramagnetic resonance) spin trapping techniques has been employed to detect these species.[48,49] LC–MS (liquid chromatography-mass spectrometry)[19] and LC–SIR (selected ion recording)–MS were employed to detect intermediates of the photocatalytic reactions for tetrabromobisphenol[50] and carbamazepine.[51] As an indirect chemical probe method, scavengers of the active species were added during the photoreaction,[22,27,49] after which the dye degradation rate was measured.

Ideally, a catalyst should be multifuncational under any environmental conditions. In the present study, we examined the adsorption and photocatalytic performance of hierarchical echinoid-like (or flower-like) BiOI with different doped concentrations of Ag and Ti for degradation of methyl orange (MO), Rhodamine B (RhB) and methylene blue (MB), which have different molecular structures and UV-visible absorption bands. We chose two different (Ag and Ti-loaded) catalytic systems for comparison. Ag was chosen because Ag^+ ion reacts with I^- of BiOI to form AgI with a band gap of ~2.8 eV[47] higher than that (~1.8 eV) of BiOI. On the other hand, Ti does not chemically react with BiOI, and TiO_2 is the most well known photocatalyst with a band gap of 3.2 eV[16]. It was reported that a higher band gap material can be combined with the lower band gap material BiOI to obtain a synergic photocatalytic effect.[1,2,4,10,11,29-31,35,36,47] The originality of this work is further discussed later. The results presented herein provide a clearer understanding of hybrid BiOI adsorption and degradation mechanisms and therefore deeper scientific insight that will be useful for the development of catalysts/adsorbents for use in water treatment facilities and environmental remediation projects.

2. Experimental Section

2.1. Catalyst preparation

Echinoid-like BiOI nanostructures were synthesized as follows. Stoichiometric amounts of $Bi(NO_3)_3·5H_2O$ (98%, Junsei, Japan) and KI (99.5%, Samchun Pure Chem., Korea) were completely dissolved in 20 mL ethylene glycol (99.5%, Samchun Pure Chem.,

Korea), after which the transparent yellow solution was transferred to a Teflon bottle that was tightly capped and placed in an oven (120ºC) for 12 hours. The final reddish-color products were fully washed with Millipore water and ethanol repeatedly, after which they were dried in an oven (80ºC) for 24 hours. We added appropriate amounts of 0.1 M silver nitrate solution (Yakuri, Japan) or titanium(IV) isopropoxide (98 %, Junsei, Japan) to dope the samples with Ag (0.1, 1.0 5.0 and 10.0 mol%) and Ti (1.0, 5.0, 10.0, 30.0 and 50.0 mol%), respectively, before adding KI, after which we followed the same procedures described above.

2.2. Catalyst characterization

The surface morphology of the powder samples was observed by scanning electron microscopy (SEM, Hitachi SE-4800). The microstructures of catalyst powder were examined by transmission electron microscopic (TEM) and high resolution TEM (HRTEM) study using a Tecnai F20 G2 FEI-TEM operated at 200.0 kV. The structural property of samples was further obtained from the electron diffraction patterns. The energy-dispersive X-ray spectroscopy (EDX) measurement was carried out to check the elemental composition of samples. Additionally, the powder X-ray diffraction (XRD) patterns were evaluated using a PANalytical X'Pert Pro MPD diffractometer with Cu Kα radiation (40 kV and 30 mA). The UV-visible absorption spectra of powder samples were obtained using a Varian Cary 5000 UV-visible-near IR (UV-Vis-NIR) spectrophotometer (Agilent Technologies). Fourier-transform infrared (FT-IR) spectra were acquired using a Thermo Scientific Nicolet iS5 spectrometer. Raman spectra of pelletized samples were recorded using a Bruker Senterra Raman spectrometer with a laser excitation energy of 758 nm. Photoluminescence spectra were collected using a SCINCO FluoroMate FS-2 at excitation wavelengths of 250 and 280 nm with a Xe lamp source. The Brunauer-Emmett-Teller (BET) surface area was measured using a Quantachrome ChemBET TPR/TPD analyzer with a thermal conductivity detector and 30% N_2/He.

2.3. Catalyst performance tests

To test the adsorption performance of the catalysts, we dispersed 10 mg of a sample into 50 mL of dye (MO, RhB and MB at 5 mg/L) solution and then measured the change

in concentration of the dye solution with time under dark conditions. Specifically, the concentration was measured based on the UV-visible absorption intensity using a Jasco V-530 UV–Vis absorption spectrophotometer. For the photocatalytic dye degradation experiments, we dispersed 10 mg of BiOI, 5mol% Ag-BiOI, or 10 mol% Ti-BiOI catalysts in a dye (MO, RhB and MB) solution (10 mg/L, 50 mL). Following adsorption of the dye for 2 hours under dark conditions, we irradiated the samples with visible (using a halogen lamp) or UV (using an UV lamp irradiating 352 nm) light. After selected irradiation times, we measured the concentration of the dye solution using a UV-visible absorption spectrophotometer (Jasco V-530). An indirect scavenger method was employed to examine the roles of active species such as •OH, $•O_2^-$ and h^+, with isopropyl alcohol (IPA), benzoquinone (BQ) and EDTA used as scavengers for •OH, $•O_2^-$ and h^+, respectively.[22,27,41,49] Following irradiation with visible ($\lambda > 420$ nm) light, we measured the UV-visible absorption of the dye solution containing the scavenger. Photoluminescence was employed to detect active •OH radicals using a terephthalic acid solution with the catalyst after visible light irradiation.[26]

3. Results and Discussion

3.1. Morphology, crystal structure and growth mechanism

Figure 1 and 2 show the SEM images of undoped, Ag-loaded (0.1, 1, 5 and 10 mol%) and Ti-loaded (1, 5, 10, 30 and 50 mol%) BiOI prepared in ethylene glycol, respectively. The SEM image of the undoped BiOI shows an echinoid-like microsphere structure with sizes of about 1 – 2 μm and a surface that appears like a connection of vertically staked walls. When 0.1 mol% Ag was loaded into BiOI, the morphology showed no critical change. However, when 1.0 mol% Ag was loaded into the BiOI, the surface changed significantly. Specifically, as Ag-loading increased, the size of the microspheres became smaller and distorted. In addition, many small clusters were shown on the surface. This change in morphology is very similar to that of AgI/BiOI hierarchical hybrid structures reported by Cheng et al.[1] Observation of the SEM images of Ti-loaded samples revealed a little change with increasing Ti-loading amount compared to Ag-loaded samples. As the Ti-

loading increased, the surface showed a wave-like structure, and the sphere size became smaller.

As shown in Figure 3, the 3D-hierarchical echinoid (or flower)-like microspheres appear to be formed by a 3D-assembly growth mechanism. In this process, small BiOI crystal units (with Ag and Ti units) are formed by a reaction of $Bi^{3+} + I^{-} + H_2O \rightarrow BiOI + 2H^{+}$. These small units initially grow into sheets that subsequently dissolve and re-grow on larger particles by making connections between vertically stacked sheets via the Ostwald ripening process.[25,52,53] The 3D-self-assembly process minimizes the surface energy required to consequently form the microspheres. The Ag or Ti units are embedded inside the 3D structure during crystal growth.

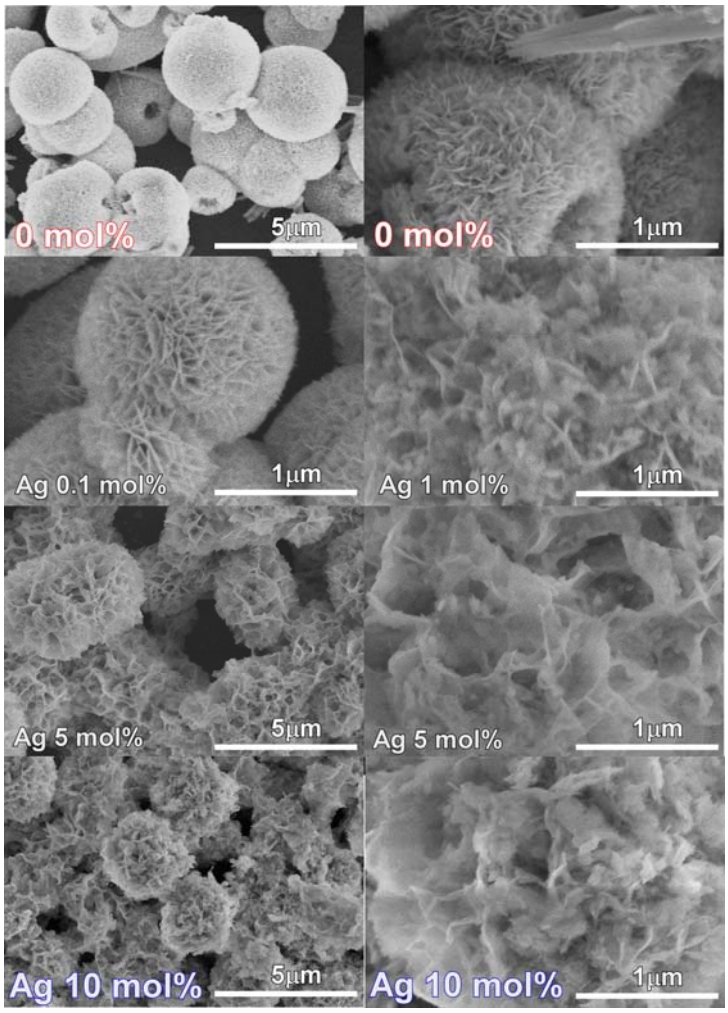

Figure 1. SEM images of BiOI doped with different concentrations (0.1, 1, 5 and 10 mol%) of Ag.

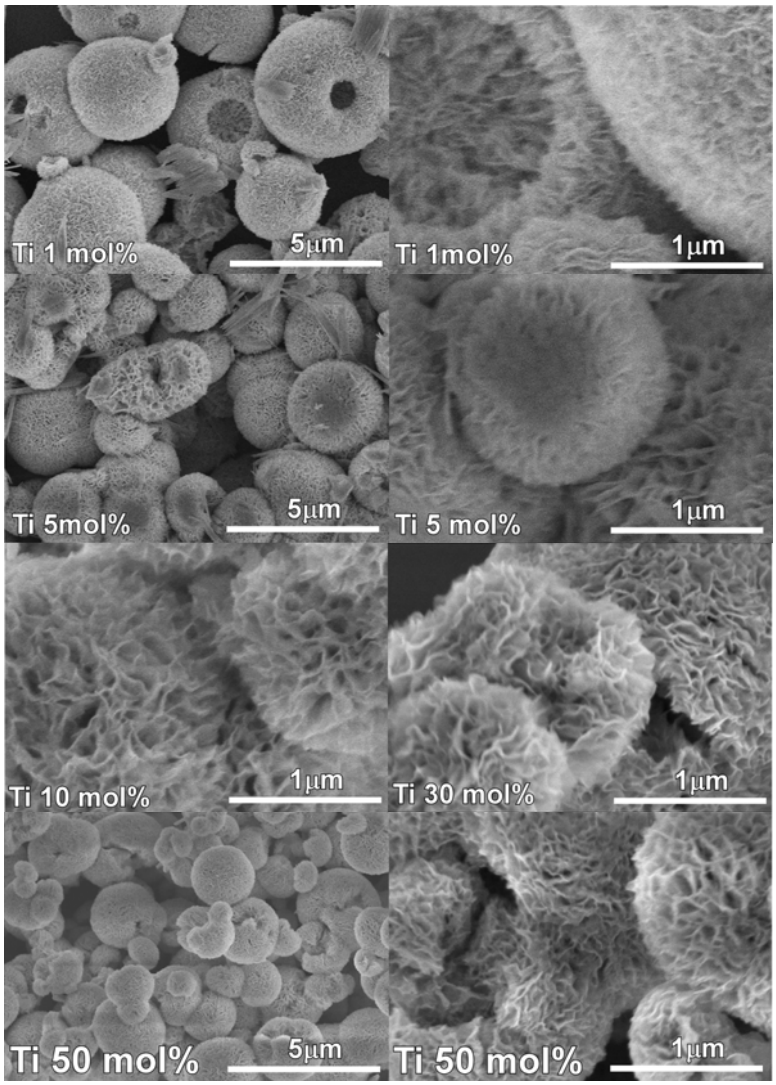

Figure 2. SEM images of BiOI doped with different concentrations (1, 5, 10, 30 and 50 mol%) of Ti.

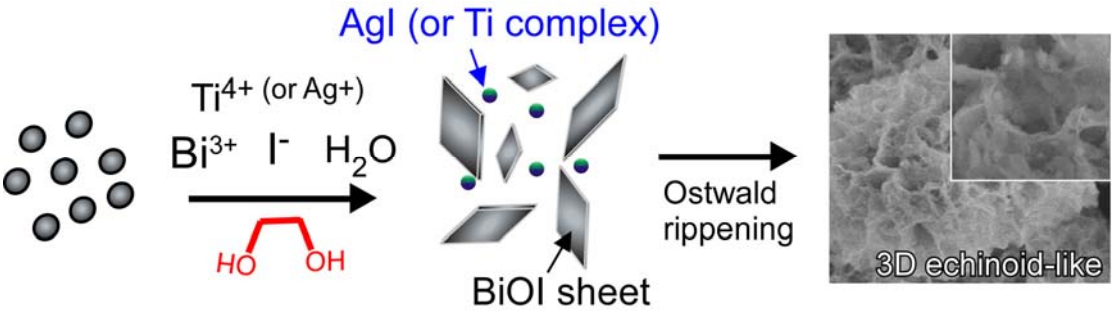

Figure 3. Plausible growth mechanism of the echinoid-like Ag and Ti-loaded BiOI nanostructures.

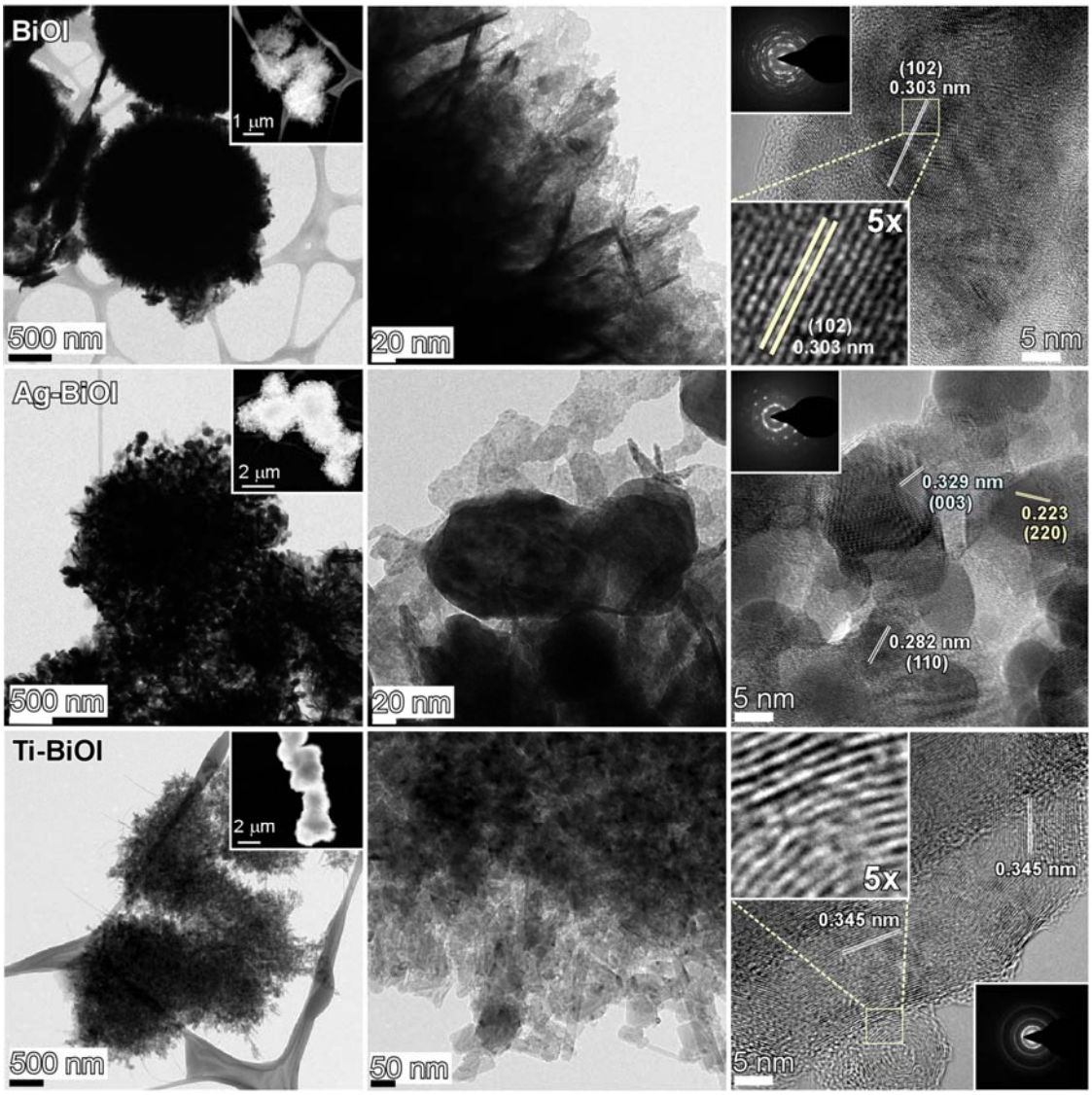

Figure 4. TEM (left and middle columns), HRTEM (right column) and high-angle annular dark field (HAADF) TEM image (inset, left column) of BiOI, Ag-BiOI (10mol%) and Ti-BiOI (50mol%) samples. Insets (right column) show the corresponding electron diffraction patterns.

We further examined the microstructures of the catalysts using TEM and HRTEM study. Figure 4 displays the TEM, HRTEM, HAADF images and the selected area electron diffraction (SAED) patterns of BiOI, Ag-BiOI (10mol%) and Ti-BiOI (50mol%) samples. The HRTEM image of BiOI showed clear lattice fringes with a spacing of 0.303 nm, corresponding to {102} facet of tetragonal BiOI. The SAED pattern also indicates

crystalline nature of the sample. For the Ag-BiOI, small clusters appear to be embedded in the microstructure as shown in the TEM image. The surface area may be decreased due to the formation of the clusters, discussed later. The HRTEM image shows the various lattice fringes with spacings of 0.282 nm, 0.329 nm and 0.223 nm. These correspond to {110} facet of BiOI, {003} facet of BiO and {220} facet of AgI, respectively. For the HRTEM image of Ti-BiOI (50mol%), interestingly the lattice spacing became wider with 0.345 nm, and the planes show a staked structure. It appears that during the crystal growth, titanium(IV) isopropoxide may incorporate between the BiOI layers to expand the lattice spacing. Furthermore, the ring SAED suggests the polycrystalline nature of sample as confirmed from the broad XRD feature (discussed later). Since the size of Ti atom is smaller than that of Bi atom Ti may easily incorporates into BiOI lattice.[54] Li et al. synthesized BiOBr–Bi_2WO_6 mesoporous nanosheet composites with and without titanium(IV) isopropoxide.[55] They found that titanium(IV) isopropoxide induces pores in the nanosheets and impacts on the facets formation.

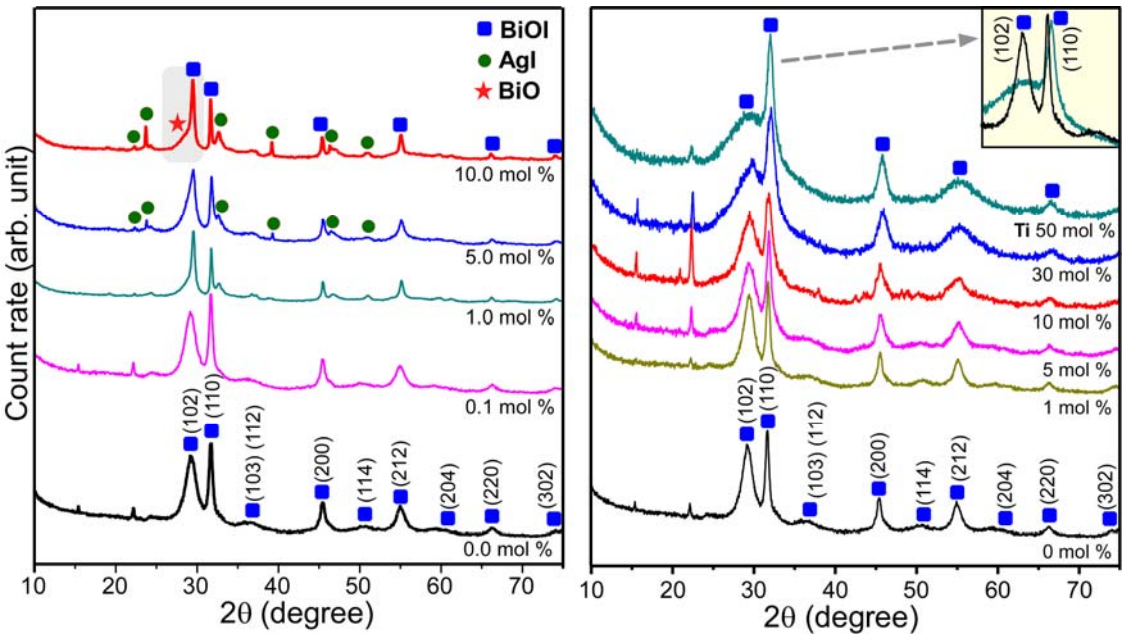

Figure 5. Power X-ray diffraction patterns of BiOI with increasing Ag (left) and Ti (right) loadings. Inset (right) shows the difference in (102) and (110) peaks between undoped BiOI and 10mol% Ti-BiOI.

Figure 5 displays the powder XRD patterns of undoped, Ag-loaded (0.1, 1, 5 and 10 mol%) and Ti-loaded (1, 5, 10, 30 and 50 mol%) BiOI prepared in ethylene glycol. The XRD patterns of the undoped flower (or echinoid)-like 3D-BiOI matched those of tetragonal (P4/nmm) BiOI (JCPDS 10-0445) well.[32,34,35,39] The four major peaks at 2θ = 29.3º, 31.8º, 45.6º and 55.1º were assigned to the (102), (110), (200) and (212) planes, respectively.[34,35,39] Other minor peaks were also assigned to the corresponding XRD peaks. As Ag-loading increased, new XRD peaks appeared, although the XRD peaks of BiOI were still predominant. The new patterns of the 10 mol% Ag-loaded BiOI matched those of hexagonal (P63mc) AgI (JCPDS 9-0374). In addition to the XRD peaks of AgI, a shoulder near the (102) peak was found, which was tentatively attributed to rhombohedral (JCPDS 1-075-0995) bismuth oxide (BiO). During the precipitation and crystal growth process, Ag^+ reacts with I^- to form AgI[1,2,4,10,11] via an ion exchange process (e.g., BiOI + $Ag^+ \rightarrow$ AgI +BiO^+). During this process, AgI is embedded in the 3D-BiOI structure. For the Ti-loaded BiOI, the XRD peak positions were very similar; however, as shown in the inset of Figure 5, some XRD peaks became much broader than others. No XRD peak of TiO_2 was observed. The (102) peak of BiOI was significantly broadened with increasing Ti amount, and the (110) peak was shifted to a larger 2θ angle. This is possibly due to the facets affected by Ti and the incorporation of Ti into BiOI lattice during crystal growth. Although, no XRD peaks were obtained from TiO_2 embedded in the lattice, EDX measurement confirms the presence of Ti (Fig. S1, Supporting Information). This suggests that the Ti is embedded in the lattice of BiOI as an amorphous form. Wei et al. prepared BiOBr-TiO_2 catalysts using tetra-butyl titanate.[54] They also did not observed XRD peaks of crystalline Ti-species, and attributed the Ti to amorphous phase.

3.2. Band gaps, Raman spectra and photoluminescence

The UV-Vis reflectance absorption spectra of the Ag-loaded (0.1, 1, 5 and 10 mol%) and Ti-loaded (1, 5, 10, 30 and 50 mol%) BiOI are displayed in Figure 6. The absorbance Y-axis data were converted from diffuse reflectance data by the Kubelka-Munk method. For the Ag-loaded samples, the absorption edge showed no critical change as the Ag amount was changed, which is in good agreement with the results reported by Lv et al.[4] However,

the edge of the Ti-loaded sample shifted to a shorter wavelength with increasing Ti. The brown color of the Ag-loaded samples remained about the same while the Ti-loaded sample became white-brown with increasing Ti. The optical band gaps were estimated using the Tauc equation, $\alpha h\nu = A(h\nu - E_g)^{n/2}$, where A is an empirical constant, and n = 1 for the direct band gap and n=4 for the indirect band gap.[2,4,9,20,56] The indirect band gaps were obtained from the intersection of the plot of $[\alpha h\nu]^{1/2}$ versus hν. For undoped BiOI, the indirect band gap was estimated to be 1.82 eV, and this value showed a small change upon Ag loading to 1.83 eV for the 10 mol% Ag-loaded BiOI. For the Ti-loaded sample, the band gap became gradually increased with increasing Ti to 1.92 eV for the 50 mol% Ti-loaded BiOI. Xia et al. reported a band gap of 1.84 eV for flower-like porous BiOI microspheres,[57] which is in good agreement with the results of the present study. A band gap of 1.76 eV for sheet-shaped single-crystalline BiOI was reported by Chang et al.[56] Band gap energies of 1.77 and 1.72 eV were reported for BiOI nanoflakes and nanoplates, respectively.[44] However, a much lower band gap of 1.46 – 1.63 eV was reported for BiOI prepared using a microwave irradiation in mannitol solution.[17]

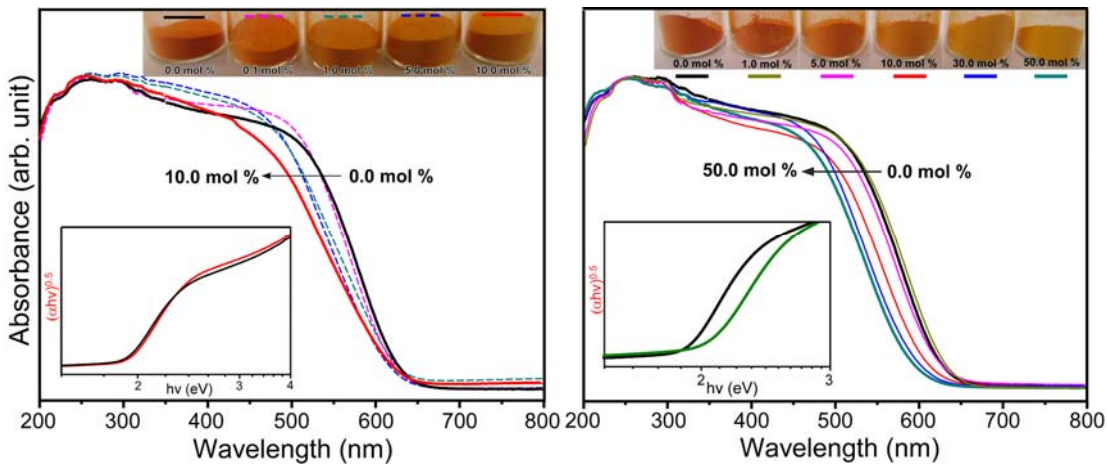

Figure 6. UV-Visible diffuse reflectance absorption spectra of BiOI with increasing Ag (left) and Ti (right) loadings. Insets (top) show the photo images of the corresponding samples. The lower left insets show the plots of $[\alpha h\nu]^{1/2}$ versus hν for BiOI, 10mol% Ag-BiOI and 50mol% Ti-BiOI.

Figure 7 displays the Raman spectra of BiOI doped with different concentrations of Ag and Ti. The corresponding FT-IR spectra are provided in the Fig. S2 of the Supporting Information. A peak at 148 cm^{-1} attributed to the E_g mode (internal Bi–I stretching) was found in all Raman spectra, which is in good agreement with previous studies.[24,27] The B_{1g} and A_{1g} modes were nearly absent. The vibrational modes of BiOI with a tetragonal structure (P4/mmm) are represented as $\Gamma = 2A_{1g} + B_{1g} + 3E_g + 2E_u + 2A_{2u}$, where A_{1g}, B_{1g}, and $3E_g$ are Raman active, and the others are IR active.[2, 12, 22,24] The major peak position showed no critical change as the amounts of Ag and Ti changed, indicating that the major BiOI structure was preserved regardless of the guests, which agrees well with the XRD results (Figure 5).

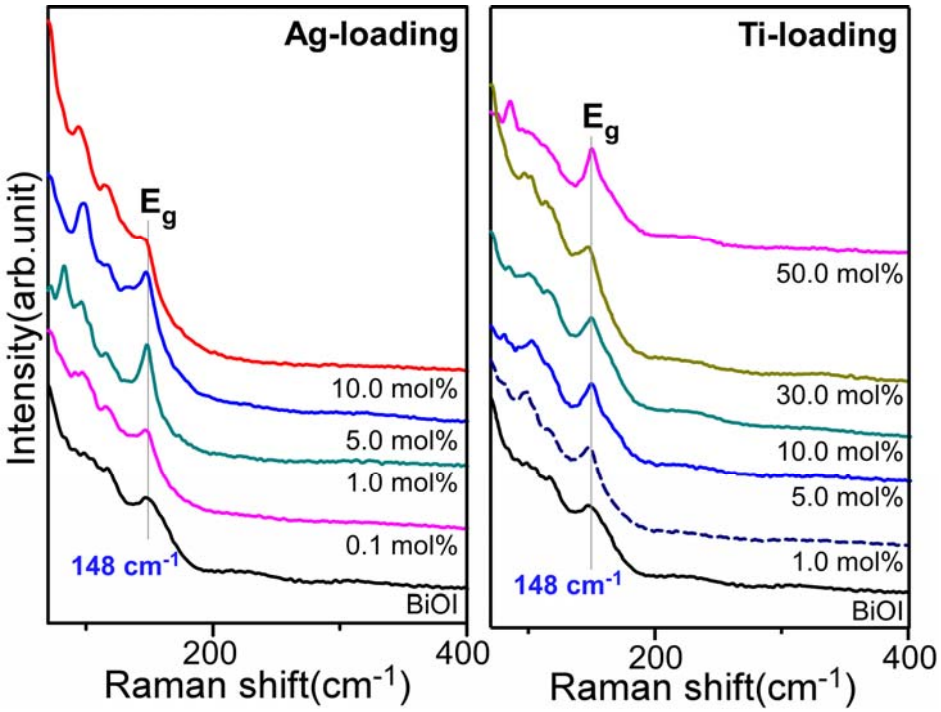

Figure 7. Raman spectra of BiOI with increasing Ag (left) and Ti (right) loadings.

Figure 8 displays the photoluminescence (PL) spectra of the BiOI, Ag and Ti-loaded BiOI catalysts at an excitation wavelength of 280 nm. A broad peak was commonly observed at around 600 nm.[32,46] Yu et al. also observed a broad peak at ~600 nm for BiOI nanoplates.[46] Photoluminescence (PL) spectroscopy has commonly been employed to predict the photocatalytic efficiency of a catalyst. Since electrons and holes play major roles in the photocatalytic reaction the catalytic activity decreases when an electron and a

hole recombine to emit a photon.[2,20,58] For this reason, catalysts with high PL will generally have lower photocatalytic performance. The PL intensity of BiOI increased by about the same amount upon Ag and Ti-loadings. Based on the PL data alone, the photocatalytic activity of the Ag and Ti-loaded BiOI should be lower; however, the observed photocatalytic activity was not consistent with the PL results, indicating that other factors are also involved in the photocatalytic mechanism.

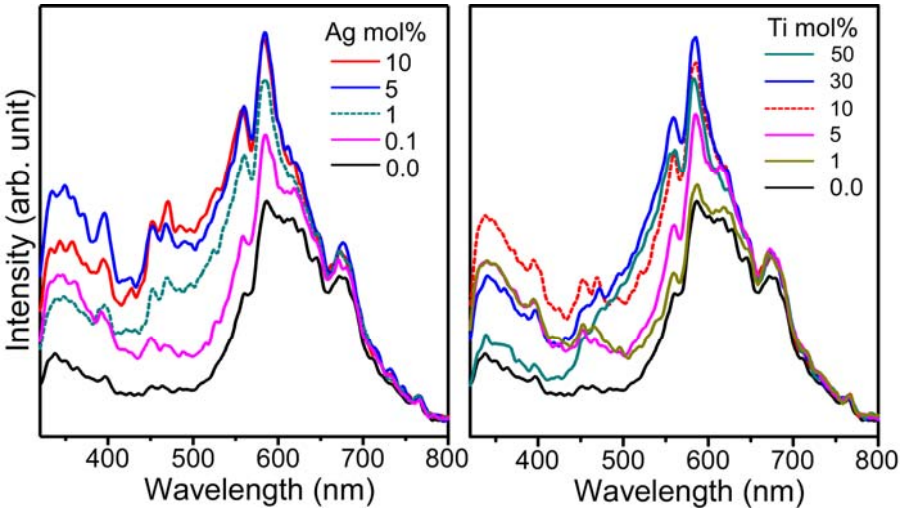

Figure 8. Photoluminescence spectra of BiOI with increasing Ag (left) and Ti (right) loadings at an excitation wavelength of 280 nm.

3.3. Adsorption of MO, RhB and MB, and BET surface area

We tested the adsorption performance of BiOI, Ag-doped BiOI and Ti-doped BiOI using methyl orange (MO), Rhodamine B (RhB) and methylene blue (MB) under dark conditions after just 10 min (Figure 9). For undoped BiOI, about 10% of MO, 90% of RhB and MB were adsorbed, which suggests that BiOI is not a suitable catalyst for MO adsorption. For 0.1 mol% Ag-doped BiOI, the adsorption performance was slightly enhanced, compared with BiOI. The adsorption performance became poor when the Ag-loading was increased above 1mol% for all the dyes i.e. MO, RhB and MB (left side, Figure 9). For the Ti-loaded BiOI with MO (top right, Figure 9), the adsorption performance was increased with increasing Ti-loading up to 30mol%. The 0.1mol% Ag doped BiOI showed highest adsorption of RhB (middle left, Figure 9). For RhB, the adsorption performance of Ti-loaded BiOI was found almost same except for 1.0mol% Ti-BiOI (middle right, Figure 9). For MB dye, the adsorption performance was lower

with 1, 5, and 10mol% Ti-BiOI, but higher with 30 and 50mol% Ti-BiOI. Among these dyes, the adsorption was commonly found to be in the order of MO << RhB < MB, which is in good consistent with the literature.[59] Zhang et al. reported that BiOBr catalysts showed better absorption performance for RhB and MB than for MO,[59] which was consistent with the results of the present study. They attributed the higher adsorption ability of RhB and MB to stronger electrostatic interactions between the dyes and the BiOBr surface. Similarly, because RhB and MB are positively charged while MO is negatively charged in solution, the negatively surface charged BiOI will interact more strongly with RhB and MB.

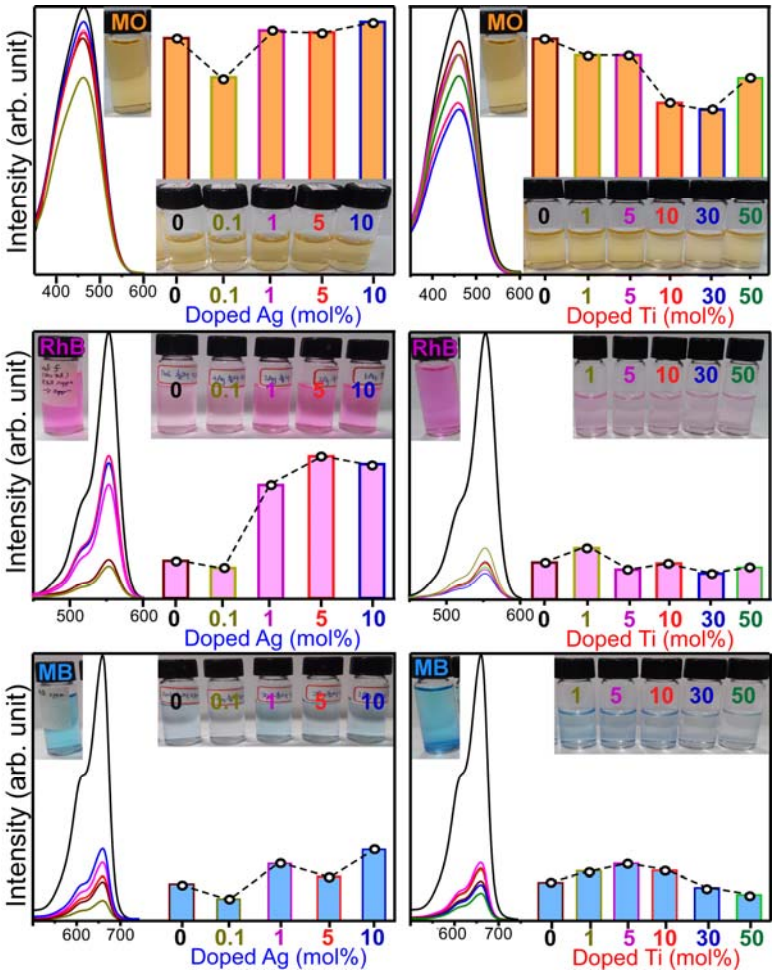

Figure 9. UV-visible absorption spectra and the corresponding peak intensities upon adsorption of MO, RhB and MB (5 mg/L, 50 mL) by 10 mg BiOI, Ag-doped BiOI and Ti-doped BiOI. Insets show the photo images of the corresponding dye solutions after adsorption. All the absorption peaks were normalized before adsorption.

Since the surface area of a catalyst is related to adsorption, BET surface areas (Fig. S3, Supporting Information) were measured. These values are summarized in Table 1 and 2 for Ag and Ti-loaded BiOI catalysts, respectively. Before loading Ag and Ti, the 3D-flower like BiOI exhibited a BET surface area of 60.8 m^2/g, which is larger than the values reported in previously conducted studies.[3,4,5,13,20,27,41,57] Xia et al. measured the BET specific surface areas of 28.3 and 5.3 for 3D flower-like BiOI and 2D-plates, respectively.[57] Upon loading 0.1% Ag into BiOI, the surface area increased slightly, while loading more than 1 mol% led to a significant decrease in BET area. For the Ti-loading below 10mol%, the surface areas were similar compared with that of undoped BiOI, while 30 and 50mol%-Ti samples showed a dramatic increase in BET surface area. Overall, for the higher loading of Ag (1, 5 and 10mol%) and Ti (30 and 50mol%), the BET surface area was correlated with the adsorption performance. In other words, the surface area effect was more dominant than other effects. For the lower Ag and Ti loadings, the adsorption of a dye onto the catalyst was more likely dependent on the nature (e.g., surface charge and molecular dipoles) of the dye and the catalyst.[59]

Table 1. BET surface areas (m^2/g) of reference (undoped) BiOI and Ag-doped BiOI with different Ag concentrations.

Ag mol%	0	0.1	1	5	10
Surface area (m^2/g)	**60.8**	**66.2**	44.3	45.1	44.2

Table 2. BET surface area (m^2/g) of reference (undoped) BiOI and Ti-doped BiOI with different Ti concentrations.

Ti mol%	0	1	5	10	30	50
Surface area (m^2/g)	**60.8**	57.8	70.5	58.0	**98.8**	**111.5**

3.4. Photocatalytic performance of MO, RhB and MB under UV and visible light

Prior to examining the detail photocatalytic performance we selected 5mol% Ag- and 10 mol% Ti-BiOI as representative test materials based on the XRD and adsorption data.

The 5mol% Ag- and 10mol% Ti-BiOI were enough to show differences in XRD and adsorption performance, compared with those of un-loaded BiOI. For the selected three catalysts, we tested the adsorption of MO, RhB and MB with a dye concentration of 10 mg/L under dark conditions (Fig. S4, Supporting Information). Upon adsorption, we examined the photodegradation of MO, RhB and MB by the three (BiOI, 5mol% Ag-BiOI and 10mol% Ti BiOI) selected catalysts under UV ($\lambda < 420$ nm) and visible ($\lambda > 420$ nm) light irradiation (Figure 10).[60] Without the catalyst, we observed no significant degradation of the dye under UV or visible light irradiation, indicating that a charge transfer process between the dye and the catalyst may be an important factor for improving dye degradation (discussed in detail below). After adsorption of the three different dyes for 2 hours in the dark, we started irradiation with UV or visible light.

Figure 10 displays the photodegradation rates (change in peak position and UV-visible absorption spectra) of MO, RhB and MB solutions with BiOI, 5mol% Ag-loaded BiOI and 10mol% Ti-loaded BiOI under UV and visible light irradiation. For MO, the degradation rate (or the change in peak position) was very similar under UV and visible irradiation. Specifically, the degradation performance showed the order of BiOI < Ag-BiOI < Ti-BiOI, and the Ti-loaded BiOI showed the best photocatalytic performance for MO dye. For RhB, the photocatalytic activity differed greatly under UV and visible irradiation. Specifically, the RhB with BiOI were efficiently degraded with time under UV irradiation, while the RhB with Ag and Ti-loaded BiOI catalysts showed very little degradation with time. The doped catalysts showed very poor photocatalytic activity for RhB under UV irradiation. However, under visible right irradiation the Ag and Ti-doped catalysts showed good photocatalytic activity comparable to or better than that of undoped BiOI. Overall, the catalytic activity was in the order of Ag-BiOI < BiOI < Ti-BiOI. Ti-loaded BiOI showed very good photocatalytic activity toward RhB under visible light irradiation, implying that the dye degradation occurs via a dye sensitized mechanism,[61,62] as discussed in detail below. In addition, the different exposed facets showed different reactivity between UV and visible light.[45] Although MB was the most efficiently adsorbed onto the catalyst surface, it was not efficiently photodegraded under UV and visible light irradiation. The peak position showed no change with time. The concentration of MB solution showed no linear decrease with irradiation time (UV and

visible) when treated with the BiOI and Ag and Ti-loaded BiOI catalysts (Fig. S5, Supporting Information), suggesting that MB dye could be removed efficiently by adsorption, but not by photocatalytic reaction. Photocatalytic performance has been shown to be more closely related to the exposed facets of a catalyst than the surface area.[43,45,63] In the dye-sensitized mechanism, a good charge transfer followed by separation is an important step, and is mainly determined by the exposed facet. The LUMO of a dye and the CB of a catalyst is another important factor for the higher charge transfer. A good interfacial wavefunction mixing (or a well-aligned energy level) promotes the charge transfer rate.

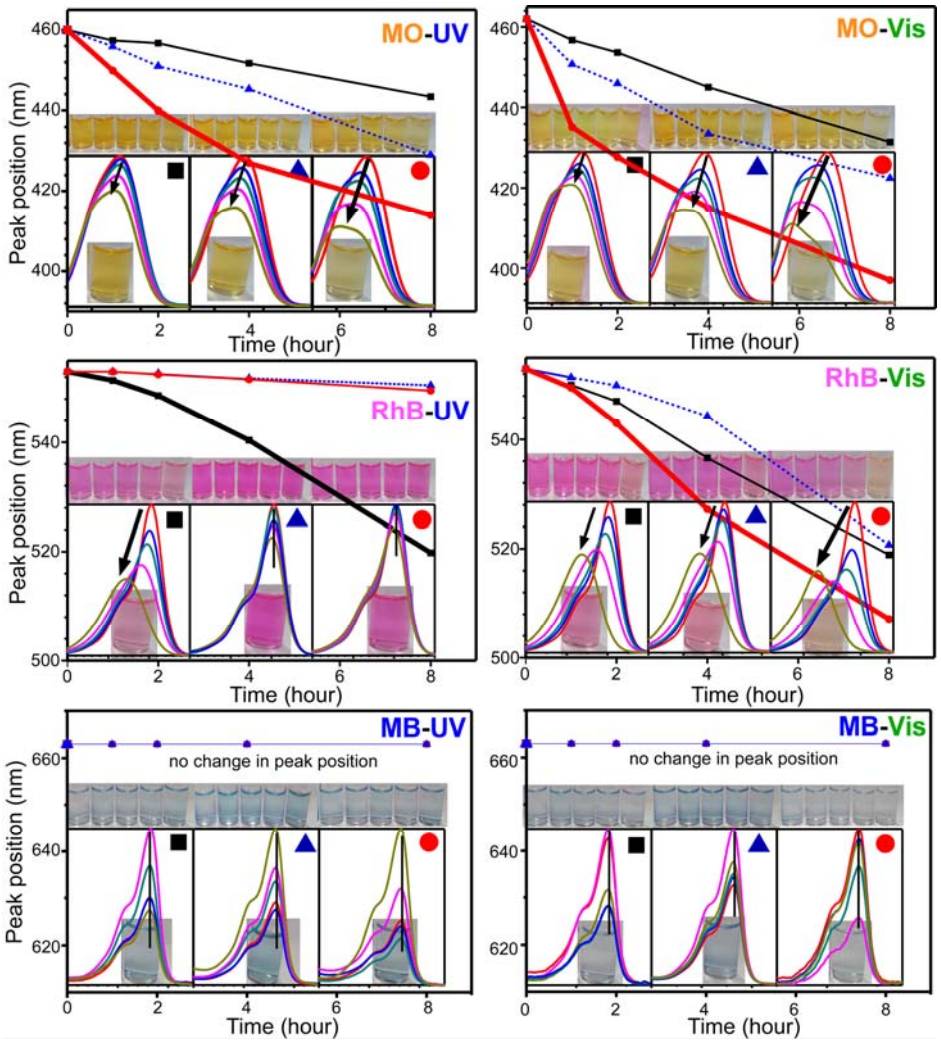

Figure 10. Photodegradation (change in peak position and UV-visible absorption spectra) of MO, RhB and MB solutions (10 mg/L, 50 mL) by BiOI(■), 5mol% Ag-loaded BiOI(▲) and 10mol% Ti-loaded BiOI (●) under UV (left column) and visible (right

column) light irradiation. Insets show the photos of the corresponding solutions with photodegradation time. The absorption wavelength of the dyes (Fig. S6, Supporting Info.) was omitted for clarity.

To clearly examine the photocatalytic mechanism and the role of active species, we employed an indirect chemical probe method using scavengers of isopropyl alcohol (IPA), benzoquinone (BQ) and EDTA for •OH, $•O_2^-$ and h^+ species, respectively. Figure 11 displays the photocatalytic degradation of RhB for BiOI, Ag(5mol%)-BiOI and Ti(50mol%)-BiOI in the absence and presence of scavengers (IPA, BQ and EDTA) under visible ($\lambda > 420$ nm) light irradiation for 6 hrs. It should be noted that the photocatalytic activity is dependent on the amount of Ag and Ti-loading. Jiang et al. prepared Ag and Ti-decorated flower-like BiOBr microspheres and found that the photocatalytic activity was highly dependent on the Ag or Ti-content.[64] The dye without a scavenger showed the greatest degradation (or the shift in peak position), with an order of Ag(5mol%)-BiOI < BiOI < Ti(50mol%)-BiOI. Upon addition of scavengers for $•O_2^-$ and h^+, the dye degradation (or the shift in peak position) was dramatically suppressed. The dye with the scavenger of $•O_2^-$ showed some degradation, but no change in absorption peak position. This indicates that other active species such as h^+ dissociates the dye without forming a secondary product (discussed later). However, the scavenger for •OH radical showed no suppression and the same degradation rate as the dye solution without a scavenger. These results indicate that the $•O_2^-$ and h^+ species are formed during visible light irradiation, and that they play important roles in dye degradation, which agrees well with the available literature.[2,3,5,14,22,19] Li et al. also found that $•O_2^-$ and h^+ species play major roles in degradation, but •OH radical showed no effect on the degradation of phenol with BiOI/$ZnSn(OH)_6$ catalyst.[5] For BiOI and Ti-BiOI catalyst, the h^+ appears to be more important than $•O_2^-$. Ye et al. reported a similar result for BiOI.[3] Furthermore, they found that $•O_2^-$ became more important than h^+ species for Pt-BiOI.[3] Similarly, in the present study, the $•O_2^-$ and h^+ species showed comparable activities for Ag-BiOI, which was attributed to an enhanced electron transfer followed by generation of $•O_2^-$.[29,30] Liu et al. used Ag/BiOI composites to degrade acid orange II, MO and RhB under visible-light irradiation and found a higher photocatalytic activity than BiOI.[29] They explained that the

electrons in the CB of BiOI accumulated on the surface of Ag and were more easily transferred to the adsorbed surface oxygen to form active $\bullet O_2^-$. Since partial degradation of RhB was found with the $\bullet O_2^-$ scavenger, we further examined the effect of BQ over the catalyst with different Ag and Ti-loadings (Figure 11). The dye degradation was found to be dependent on the Ag or Ti-content. The BiOI with higher loadings of Ag (1, 5 and 10mol%) showed poor degradation, compared with undoped and 0.1mol% Ag-doped BiOI. On the other hand, Ti-BiOI catalysts showed better photodegradation performance as discussed in Figure 10 for RhB under visible light irradiation.

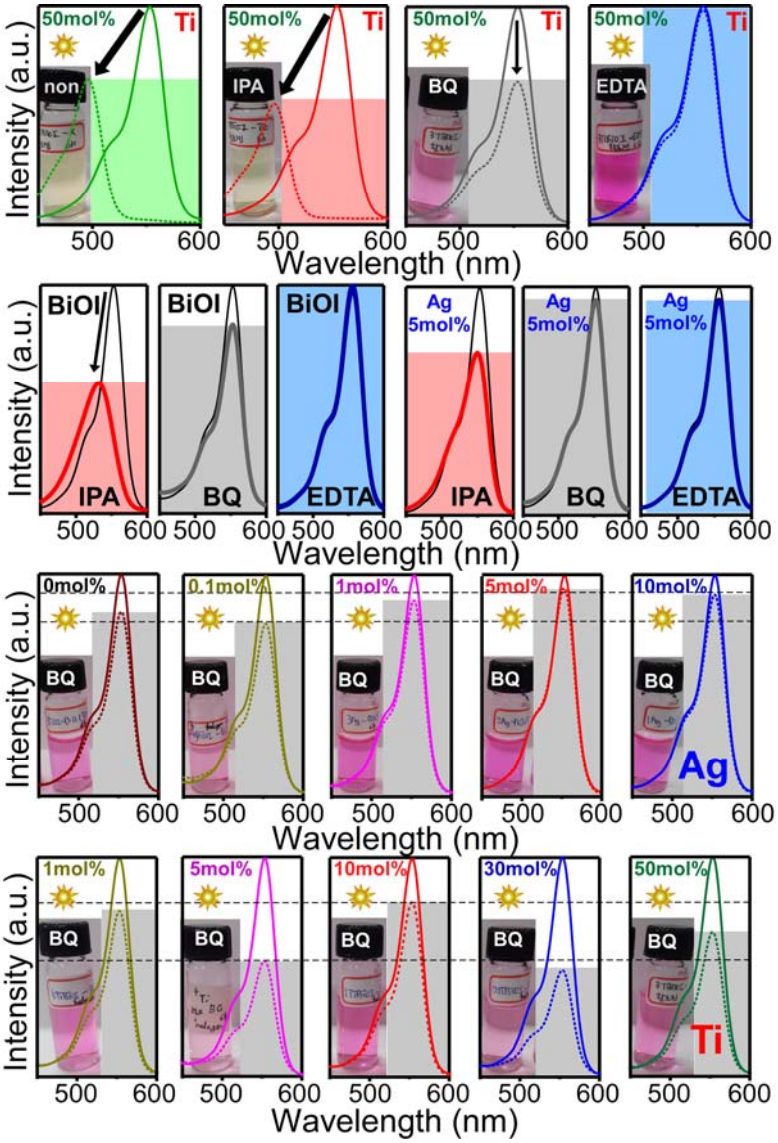

Figure 11. Photocatalytic degradation (top two lines) of RhB with BiOI, Ag(5mol%)-BiOI and Ti(50mol%)-BiOI in the absence and presence of scavengers (IPA, BQ and

EDTA) under visible light irradiation for 6 hrs. Photocatalytic degradation (bottom two lines) of RhB over Ag-BiOI and Ti-BiOI with different Ag and Ti-loaded BiOI in the presence of BQ under visible light irradiation for 6 hrs.

To confirm that •OH had no effect on the dye degradation, we employed photoluminescence spectroscopy using terephthalic acid.[27,20,22,51] When •OH radicals are formed in response to visible light irradiation they react with terephthalic acid to form luminescent (λ_{em} = 425 nm) 2-hydroxyterephthalic acid. We observed no significant emission signal (Fig. S7, Supporting Information) at 425 nm for the BiOI, Ag(10%)-BiOI or Ti(5%)-BiOI catalysts after visible light irradiation or UV irradiation for 6 hrs, confirming that no significant •OH radical was produced during the photoirradiation, and that it was not involved in the photodegradation reaction. For Bi_2S_3/BiOI catalyst under visible light irradiation, Cao et al. observed a photoluminescence peak at 425 nm, which was attributed to the formation of •OH radical.[27] However, they found that the •OH radical effect was not as strong as that of the $\bullet O_2^-$ and h^+ species for the degradation of MO.

We further examined the photodegradation of BiOI with different amount of Ag and Ti-loadings without adding any scavengers. Figure 12 shows that 0.1mol% Ag-BiOI is the most efficient catalyst for RhB dye degradation and shift in absorbance position of dye solution. However, BiOI with 1, 5 and 10mol% Ag showed poor degradation and smaller shift in peak position. This indicates that RhB is poorly degraded when the amount of Ag was loaded above 1mol%. Lu et al. prepared Ag-modified (0.2–2.0wt%) BiOBr catalyst and tested photodegradation of RhB under visible light.[65] They found similar catalytic behaviour for pure BiOBr with higher catalytic activity than that of Ag-modified BiOBr. They attributed the poor performance from Ag-modified BiOBr to formation of Ag_2O. However, Kong et al. found an enhanced photocatalytic performance with loadings below 0.5wt% AgBr, and poor performance above 1.0wt% AgBr, compared with pure BiOBr.[66]

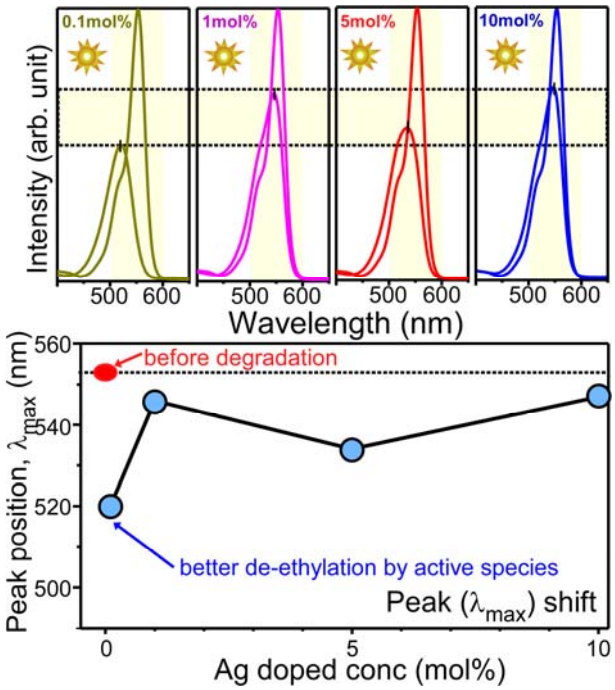

Figure 12. Photocatalytic degradation (and the change in peak position) of RhB over BiOI with Ag-loading under visible light irradiation for 6 hrs. The UV-visible absorption peaks were normalized before photoirradiation.

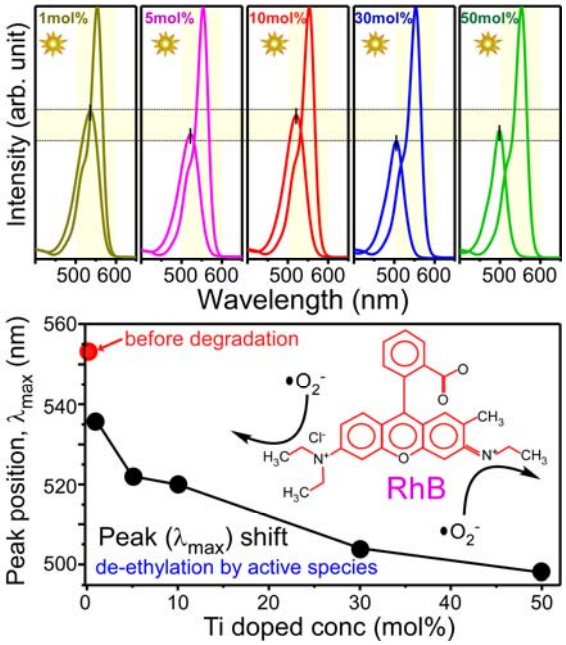

Figure 13. Photocatalytic degradation (and the change in peak position) of RhB over BiOI with different Ti-loadings under visible light irradiation for 6 hrs. The UV-Vis. absorption peaks were normalized before photoirradiation.

For the Ti-loaded BiOI (Figure 13), the UV-visible absorption intensity showed no linear relationship with the Ti-amount. However, the blue shift in peak position was linearly increased with increasing the Ti-amount. This indicates that $\bullet O_2^-$ radical became more important as the Ti-amount was increased in BiOI. The $\bullet O_2^-$ radical may attack the *N*-ethyl group of RhB (as shown in the inset of Figure 13) to initially form secondary products, which results in the blue-shift in absorption position.[67]

Based on the aforementioned results, the following photodegradation mechanism was proposed[27,43] under visible (λ >420 nm) light irradiation for BiOI and doped BiOI (Figure 14).

$$\text{Dye} + \text{Visible light} \rightarrow \text{Dye}\,(e^-_{CB} + h^+_{VB}) \quad (1)$$

$$\text{adsorbed Dye}\,(e^-_{CB} + h^+_{VB}) + \text{BiOI} \rightarrow \text{BiOI}\,(e^-_{CB}) + \text{Dye}\,(h^+_{VB}) \quad (2)$$

$$\text{BiOI} + \text{UV and visible light} \rightarrow \text{BiOI}\,(e^-_{CB} + h^+_{VB}) \quad (3)$$

$$\text{BiOI}\,(e^-_{CB}) + \text{adsorbed } O_2 \text{ (or surface O)} \rightarrow \bullet O_2^- \text{ (or } \bullet O^-) + \text{BiOI} \quad (4)$$

$$H_2O \rightarrow H^+ + OH^- \quad (5)$$

$$\bullet O_2^- \text{ (or } \bullet O^-) + H^+ \rightarrow \bullet O_2H \text{ (or } \bullet OH) \quad (6)$$

$$OH^- + \text{BiOI}\,(h^+_{VB}) \rightarrow \bullet OH \quad (7)$$

$$H_2O + \text{BiOI}\,(h^+_{VB}) \rightarrow H^+ + \bullet OH \quad (8)$$

$$\bullet O_2^-,\ h^+ \text{ or } \bullet OH + \text{adsorbed Dye/Dye}^+ \rightarrow \text{degradation products} \quad (9)$$

When a dye absorbs visible light, an electron (e^-) and a hole (h^+) are created in the conduction and valence bands (CB and VB), respectively. In a dye sensitized mechanism,[22,61,62] the electron in the CB transfers to the CB of the catalyst before being recombined with a hole (Figure 14). The transfer rate is determined by good interfacial wavefunction mixing (and good adsorption) between the dye and the catalyst. Based on the UV-Vis absorption spectra (Figure 6), the catalyst could directly absorb UV or visible light to create e^- and h^+ in the CB and VB, respectively. The electron in the CB of the catalyst is captured by the adsorbed molecular (or atomic) oxygen to form $\bullet O_2^-$ (or $\bullet O^-$) radicals, which degrade the adsorbed dye.[30] As shown in Figure 11, the $\bullet O_2^-$ scavenger suppressed dye degradation. Additionally, oxygen vacancies have been shown to play active roles in dye degradation.[68] The electron in the energy state of oxygen vacancy was trapped by the surface oxygen to create active $\bullet O_2^-$, and the $\bullet O_2^-$ radical may have

proceeded to form active •OH radicals. The adsorbed OH^- species may also capture the hole in the VB of BiOI to form •OH radicals.[51,59] However, the •OH radical was not involved in the dye degradation because there was no •OH scavenger effect and no PL emission of 2-hydroxyterephthalic acid. The h^+_{VB} in the catalyst or in the dye acts as an active species to finally degrade the dye,[47] as confirmed by the hole scavenger test. Consequently, O_2^- and h^+ species primarily degrade the dye, which is consistent with the available literature.[2,3,5]

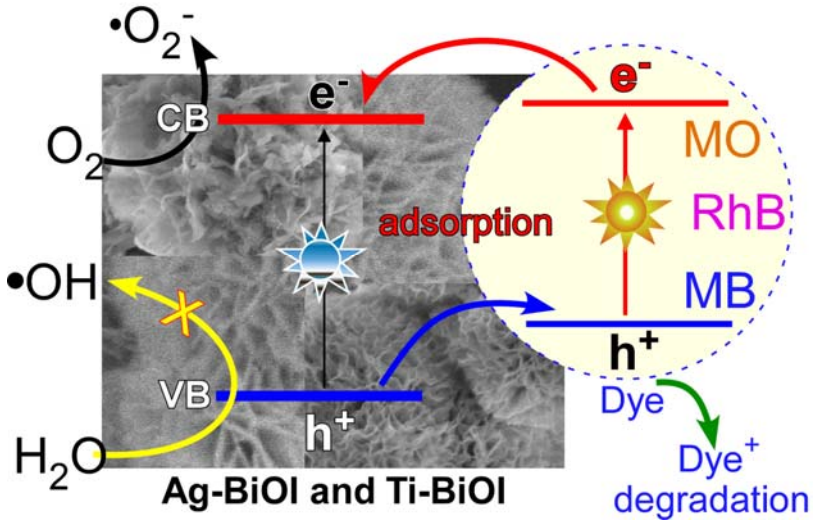

Figure 14. Photocatalytic degradation mechanism of a dye over the catalysts.

Table 3. Summary of literatures using similar catalyst systems.

Catalysts	Experimental conditions	Test systems and performances
AgI (16–400 nm) /BiOI[1]	BiOI in $AgNO_3$ EG solution, ion exchange	2,4-dichlorophenol, under Vis., enhanced
AgI(15.7,28.2,35.2, 47.0, 70.4%)/BiOI microspheres[2]	BiOI in $AgNO_3$ aq. solution, ion exchange	RhB and phenol under Vis., enhanced, max at 70.4% AgI
AgI(10, 40, 60%)/BiOI[4]	BiOI in $AgNO_3$ aq. solution	MO, RhB, MB under Vis., enhanced (best at 40%, and MB> RhB > MO)
AgI(0-100%)/BiOI[47]	Bi nitrate + $AgNO_3$ + KI in EtOH/H_2O (85°C, 2hrs)	MO and phenol enhanced compared with BiOI, best at 20% AgI
Ag/BiOI	BiOI in $AgNO_3$ sol. and UV	acid orange II, MO, RhB

(0.3, 0.6, 0.9 %)[29]	photoirradiation	under Vis., enhanced, best at 0.6 %
Ag/BiOI (1.1, 2.1, 4.5, 8.0%)[30]	BiOI in $AgNO_3$ sol. and photoirradiation	E. coli 8099, under Vis., enhanced, best at 4.5%
Ag/AgI/BiOI[10]	BiOI in $AgNO_3$ aq. sol., photoirradiation	MB and o-nitrophenol, under Vis., enhanced
Ag/AgI/BiOI[11]	BiOI in $AgNO_3$ EtOH/H_2O sol., photoirradiation	MO, under Vis., enhanced
TiO_2(0-100%)/BiOI[31]	Bi nitrate + tetrabutyl titanate aq. sol.: reverse microemulsions.	MO, enhanced, best at 25%, under Vis.
BiOI-coated on TiO_2 nanotube wall[35]	Impregnating-hydroxylation method using BiI_3	MO, under Vis., enhanced,
TiO_2(1-2%, 50%)/BiOI[36]	Bi nitrate (EG) + $AgNO_3$ (EG) + TiO_2 (H_2O)	Phenol under Vis., best at 25%
echinoid-like BiOI, AgI/BiOI and Ti-BiOI microspheres (***this work***)	Bi nitrate + $AgNO_3$ (or Ti isopropoxide) + KI in EG (120°C, 12hrs)	MO, RhB, MB under UV and Vis.

Finally, to emphasize the originality and new results of the present study, we summarized the literatures using similar catalysts in Table 3. The AgI/BiOI (or Ag/BiOI) catalysts were commonly synthesized as follows: BiOI was first synthesized and then dispersed in $AgNO_3$ solution.[1,2,4,10,11,29,30] AgI was formed at the interface by an ion exchange reaction. However, we mixed Bismuth nitrate, $AgNO_3$ (or Ti isopropoxide) and KI together in EG, and treated at 120°C for 12hrs. Although Cheng et al. synthesized AgI/BiOI using a similar method, but used a mixed EtOH/H_2O solvent, and thermal-treated at 85°C for 2hrs.[47] They examined photodegradation of MO and phenol under visible light irradiation, and found an enhanced catalytic performance upon Ag-loading, consistent with out result for MO. However, we further examined RhB and MB under UV light as well as visible light, and the new results were discussed earlier. There was no report on the photocatalytic study performed under UV light with the loaded BiOI. The Ti-BiOI catalyst was synthesized differently in the present work, and carefully tested for MO, RhB and MB which have different molecular structures and UV-visible absorption bands. The Ti-loading enhances the catalytic performance for MO under UV and visible

light. For RhB, the Ti-loading showed an enhanced effect under visible light, but poor performance under UV light, compared with un-loaded BiOI.

4. Conclusion

Echinoid flower-like BiOI with various concentrations of Ag (0.1, 1.0, 5.0, 10.0 mol%) and Ti (1.0, 5.0, 10.0, 30.0, 50.0 mol%) was successfully synthesized in an ethylene glycol environment and their fundamental properties were examined by SEM, XRD, UV-visible absorption, Raman, FT-IR, photoluminescence and BET surface area measurements. The adsorption and photocatalytic performances were demonstrated for MO, RhB and MB. The adsorption performance was mainly related to the nature of the dye and the catalyst surface structure, not the surface area.

New important findings of the present study are as follows:

1) MB was commonly the most efficiently adsorbed by the catalysts, while none of the catalysts adsorbed MO well. Overall, the adsorption was found to be in the order of MO << RhB < MB, which was attributed to electrostatic interactions between the dye and the catalyst surface.

2) MO was efficiently photodegraded by the catalysts under UV and visible lights in the order of BiOI < Ag-BiOI < Ti-BiOI. For RhB, BiOI was an efficient photocatalyst under UV irradiation, while Ag and Ti-loaded BiOI showed poor photocatalytic activity. Under visible light irradiation, the catalysts showed good catalytic activity with an order of Ag-BiOI < BiOI < Ti-BiOI. MB showed poor photodegradation with the catalysts under both UV and visible light irradiation.

3) A dye sensitized mechanism was proposed in which light absorption by the dye followed by a charge transfer from the dye to the catalyst is involved. The active species of $\bullet O_2^-$ and h^+ (more active) play important roles in the photocatalytic process. It was found that the $\bullet O_2^-$ species initially create secondary dissociation products, while h^+ species showed a total dissociation without forming any secondary product. The photocatalytic activity was understood by various factors such as surface area, crystallinity, good interfacial wavefunction mixing (or the well-aligned energy level for change transfer), and the relative role of active species.

The present study provides new insight that can aid in selection of an appropriate adsorbent/catalyst for pollutant removal by explaining the adsorption and photodegradation mechanism of MO, RhB and MB with BiOI and Ag and Ti-BiOI catalysts under UV and visible light irradiation.

Acknowledgements. This work was financially supported by the India-Korea joint project, the National Research Foundation of Korea (NRF) grant funded by the Korean government (MEST) (NRF-2012-0006296), and the Department of Science and Technology, New Delhi through the Indo-Korea/P-02 grant.

References

1. H. Cheng, W. Wang, B. Huang, Z. Wang, J. Zhan, X. Qin, X. Zhang and Y. Dai, *J. Mater. Chem. A*, 2013, **1**, 7131–7136.

2. L. Chen, D. Jiang, T. He, Z. Wu and M. Chen, *CrystEngComm*, 2013, **15**, 7556–7563.

3. L. Ye, X. Liu, Q. Zhao, H. Xie and L. Zan, *J. Mater. Chem. A*, 2013, **1**, 8978–8983.

4. Y. Lv, H. Liu, W. Zhang, S. Ran, F. Chi, B. Yang and A. Xia, *J. Env. Chem. Eng.*, 2013, **1**, 526–533.

5. H. Li, Y. Cui, W. Hong and B. Xu, *Chem. Eng. J.*, 2013, **228**, 1110–1120.

6. H. Li, Y. Cui and W. Hong, *Appl. Surf. Sci.*, 2013, **264**, 581–588.

7. D. K. Ma, S. M. Zhou, X. Hu, Q. R. Jiang and S. M. Huang, *Mater. Chem. Phys.*, 2013, **140**, 11–15.

8. X. Qin, H. Cheng, W. Wang, B. Huang, X. Zhang and Y. Dai, *Mater. Lett.*, 2013, **100**, 285–288.

9. J. Cao, C. Zhou, H. Lin, B. Xu and S. Chen, *Mater. Lett.*, 2013, **109**, 74–77.

10. T. Li, S. Luo and L. Yang, *Mater. Lett.*, 2013, **109**, 247–252.

11. J. Cao, Y. Zhao, H. Lin, B. Xu and S. Chen, *J. Solid State Chem.*, 2013, **206**, 38–44.

12. H. Li, Q. Jia, Y. Cui and S. Fan, *Mater. Lett.*, 2013, **107**, 262–264.

13. J. Cao, B. Xu, H. Lin and S. Chen, *Chem. Eng. J.*, 2013, **228**, 482–488.

14. L. Ye, J. Chen, L. Tian, J. Liu, T. Peng, K. Deng and L. Zan, *Appl. Catal. B*, 2013, **130–131**, 1–7.

15. Y. Lei, G. Wang, P. Guo and H. Song, *Appl. Surf. Sci.*, 2013, **279**, 374–379.

16. Y. Wu, Z. Zhou, Y. Tuo, Y. Huang and S. Shen, *Mater. Lett.*, 2013, **111**, 43–46.

17. G. Li, F. Qin, R. Wang, S. Xiao, H. Sun and R. Chen, *J. Colloid Interface Sci.*, 2013, **409**, 43–51.

18. Z. Cui, M. Si, Z. Zheng, L. Mi, W. Fa and H. Jia, *Catal. Commun.*, 2013, **42**, 121–124.

19. C. Chang, L. Zhu, Y. Fu and X. Chu, *Chem. Eng. J.*, 2013, **233**, 305–314.

20. K. H. Reddy, S. Martha and K. M. Parida, *Inorg. Chem.*, 2013, **52**, 6390–6401.

21. M. Su, C. He, L. Zhu, Z. Sun, C. Shan, Q. Zhang, D. Shu, R. Qiu and Y. Xiong, *J. Hazard. Mater.*, 2012, **229–230**, 72–82.

22. J. Cao, B. Xu, H. Lin, B. Luo and S. Chen, *Chem. Eng. J.*, 2012, **185**, 91–99.

23. R. Hao, X. Xiao, X. Zuo, J. Nan and W. Zhang, *J. Hazard. Mater.*, 2012, **209–210**, 137–145.

24. F. Dong, Y. Sun, M. Fu, Z. Wu and S. C. Lee, *J. Hazard. Mater.*, 2012, **219–220**, 26–24.

25. K. Ren, K. Zhang, J. Liu, H. Luo, Y. Huang and X. Yu, *CrystEngComm*, 2012, **14**, 4384–4390.

26. X. Xiao, R. Hao, M. Liang, X. Zuo, J. Nan, L. Li and W. Zhang, *J. Hazard. Mater.*, 2012, **233–234**, 122–130.

27. J. Cao, B. Xu, H. Lin, B. Luo and S. Chen, *Dalton Trans.*, 2012, **41**, 11482–11490.

28. L. Chen, S. F. Yin, S. L. Luo, R. Huang, Q. Zhang, T. Hong and P. C. T. Au, *Ind. Eng. Chem. Res.*, 2012, **51**, 6760–6768.

29. H. Liu, W. Cao, Y. Su, Y. Wang and X. Wang, *Appl. Catal. B*, 2012, **111-112**, 271–279.

30. L. Zhu, C. He, Y. Huang, Z. Chen, D. Xia, M. Su, Y. Xiong, S. Li and D. Shu, *Sepa. Puri. Technol.*, 2012, **91**, 59–66.

31. Z. Liu, X. Xu, J. Fang, X. Zhu, J. Chu and B. Li, *Appl. Surf. Sci.*, 2012, **258**, 3771–3778.

32. X. Shi, X. Chen, X. Chen, S. Zhou and S. Lou, *Mater. Lett.*, 2012, **68**, 296–299.

33. N. T. Hahn, S. Hoang, J. L. Self and C. B. Mullins, *ACS Nano*, 2012, **6**, 7712–7722.

34. L. Song, S. Zhang, and Q. Wei, *Ind. Eng. Chem. Res.*, 2012, **51**, 1193–1197.

35. G. Dai, J. Yu and G. Liu, *J. Phys. Chem. C*, 2011, **115**, 7339–7346.

36. Y. Li, J. Wang, B. Liu, L. Dang, H. Yao and Z. Li, *Chem. Phys. Lett.*, 2011, **508**,

102–106.

37. J. Cao, B. Xu, B. Luo, H. Lin and S. Chen, *Catal. Commun.*, 2011, **13**, 63–68.

38. Y. Li, J. S. Wang, H. C. Yao, L. Y. Dang and Z. J. Li, *Catal. Commun.*, 2011, **12**, 660–664.

39. M. Liu, L. Zhang, K. Wang and Z. Zheng, *CrystEngComm*, 2011, **13**, 5460–5466.

40. J. Jiang, X. Zhang, P. Sun and L. Zhang, *J. Phys. Chem. C*, 2011, **115**, 20555–20564.

41. T. B. Li, G. Chen, C. Zhou, Z. Y. Shen, R. C. Jin and J. X. Sun, *Dalton Trans.*, 2011, **40**, 6751–6758.

42. Z. Jia, F. Wang, F. Xin, and B. Zhang, *Ind. Eng. Chem. Res.*, 2011, **50**, 6688–6694.

43. Y. Li, J. Wang, H. Yao, L. Dang and Z. Li, *J. Mol. Catal. A*, 2011, **334**, 116–122.

44. Y. Wang, K. Deng, and L. Zhang, *J. Phys. Chem. C*, 2011, **115**, 14300–14308.

45. L. Ye, L. Tian, T. Peng and L. Zan, *J. Mater. Chem.*, 2011, **21**, 12479–12484.

46. C. Yu, J. C. Yu, C. Fan, H. Wen and S. Hu, *Mater. Sci. Eng. B*, 2010, **166**, 213–219.

47. H. Cheng, B. Huang, Y. Dai, X. Qin and X. Zhang, *Langmuir*, 2010, **26**, 6618–6624.

48. Y. Chen, D. Li, X. Wang, L. Wu, X. Wang and X. Fu, *New J. Chem.*, 2005, **29**, 1514–1519.

49. M. Yin, Z. Li, J. Kou and Z. Zou, *Environ. Sci. Technol.*, 2009, **43**, 8361–8366.

50. J. Xu, W. Meng, Y. Zhang, L. Li and C. Guo, *Appl. Catal. B*, 2011, **107**, 355–362.

51. J. Xu, L. Li, C. Guo, Y. Zhang and W. Meng, *Appl. Catal. B*, 2013, **130–131**, 285–292.

52. G. Jiang, X. Wang, Z. Wei, X. Li, X. Xi, R. Hu, B. Tang, R. Wang, S. Wang, T. Wang and W. Chen, *J. Mater. Chem. A*, 2013, **1**, 2406–2410.

53. L. P. Zhu, G. H. Liao, N. C. Bing, L. L. Wang, Y. Yang and H. Y. Xie, *CrystEngComm*, 2010, **12**, 3791–3796.

54. X.-X. Wei, H. Cui, S. Guo, L. Zhao and W. Li, *J. Hazard. Mater.*, 2013, **263**, 650-658

55. Y. Li, Y. Liu, J. Wang, E. Uchaker, Q. Zhang, S. Sun, Y. Huang, J. Li and G. Cao, *J. Mater. Chem. A*, 2013, **1**, 7949-7956.

56. X. Chang, J. Huang, C. Cheng, Q. Sui, W. Sha, G. Ji, S. Deng and G. Yu, *Catal. Commun.*, 2010, **11**, 460–464.

57. J. Xia, S. Yin, H. Li, H. Xu, L. Xua and Q. Zhang, *Colloids Surf. A*, 2011, **387**, 23–28.

58. D. Zhang, M. Wen, B. Jiang, G. Li and J. C. Yu, *J. Hazard. Mater.*, 2012, **211–212**, 104–111.

59. D. Zhang, J. Li, Q. Wang and Q. Wu, *J. Mater. Chem. A*, 2013, **1**, 8622–8629.

60. Y. Lei, C. Zhang, H. Lei and J. Huo, *J. Colloid Interface. Sci.*, 2013, **406**, 178–185.

61. B. Subash, B. Krishnakumar, M. Swaminathan and M. Shanthi, *Langmuir*, 2013, **29**, 939–949.

62. Y. F. Fang, W. H. Ma, Y. P. Huang and G. W. Cheng, *Chem. Eur. J.*, 2013, **19**, 3224–3229.

63. N. Roy, Y. Sohn and D. Pradhan, *ACS Nano*, 2013, **7**, 2532–2540.

64. G. Jiang, R. Wang, X. Wang, X. Xi, R. Hu, Y. Zhou, S. Wang, T. Wang and W. Chen, *ACS Appl. Mater. Interfaces*, 2012, **4**, 4440–4444.

65. L. Lu, L. Kong, Z. Jiang, H. H.-C. Lai, T. Xiao and P.P. Edwards, *Catal. Lett*., 2012 **142**, 771–778.

66. L. Kong, Z. Jiang, H. H. Lai, R. J. Nicholls, T. Xiao, M. O. Jones and P. P. Edwards, *J. Catal.*, 2012, **293**, 116-125.

67. Z. Jia, F. Wang, F. Xin and B. Zhang, *Ind. Eng. Chem. Res*., 2011, **50**, 6688-6694.

68. L. Ye, K. Deng, F. Xu, L. Tian, T. Peng and L. Zan, *Phys. Chem. Chem. Phys.*, 2012, **14**, 82–85.

Adsorption and UV/visible photocatalytic activity of echinoid-like Ag and Ti-loaded BiOI were tested for methyl orange, Rhodamine B and methylene blue.